Inter- and Intrahemispheric Sources of Vestibular Signals to V1

Guy Bouvier[1,2,3,*,#], Alessandro Sanzeni[4,5,6,*], Elizabeth Hamada[7], Nicolas Brunel[4,6], & Massimo Scanziani[1,2,#]

Affiliations

[1] Department of Physiology, University of California, San Francisco, San Francisco, CA, USA
[2] Howard Hughes Medical Institute, University of California, San Francisco, San Francisco, CA, USA
[3] Université Paris-Saclay, CNRS, Institut des Neurosciences Paris-Saclay, 91400 Saclay, France
[4] Department of Computing Sciences, Bocconi University, 20100 Milan, Italy
[5] Center for Theoretical Neuroscience and Mortimer B Zuckerman Mind Brain Behavior Institute, Columbia University, New York, NY 10027, USA
[6] Department of Neurobiology, Duke University, Durham, NC 27710, USA
[7] Department of Neurology, University of California, San Francisco, San Francisco, CA, USA

* The authors contributed equally to this work.

[#] Corresponding authors : massimo@uscf.edu and guy.bouvier@cnrs.fr

Abstract

Head movements are sensed by the vestibular organs. Unlike classical senses, signals from vestibular organs are not conveyed to a dedicated cortical area but are broadcast throughout the cortex. Surprisingly, the routes taken by vestibular signals to reach the cortex are still largely uncharted. Here we show that the primary visual cortex (V1) receives real-time head movement signals — direction, velocity, and acceleration — from the ipsilateral pulvinar and contralateral visual cortex. The ipsilateral pulvinar provides the main head movement signal, with a bias toward contraversive movements (e.g. clockwise movements in left V1). Conversely, the contralateral visual cortex provides head movement signals during ipsiversive movements. Crucially, head movement variables encoded in V1 are already encoded in the pulvinar, suggesting that those variables are computed subcortically. Thus, the convergence of inter- and intrahemispheric signals endows V1 with a rich representation of the animal's head movements.

Introduction

Many of the sensory organs that enable us to perceive the world around us are located in our head; for example, the eyes. To accurately represent our surroundings, sensory systems in the brain must combine their primary source of sensory information, e.g. visual signals, with information about head movements in space[1,2]. The vestibular organs, located in the inner ear, provide this information by transforming head movement into neural signals. Unlike other senses, however, these head movement signals are not processed by a dedicated cortical area, but are instead broadcast throughout the brain[3–9]. Previous studies in rodents have demonstrated that neurons in primary sensory areas such as the primary visual cortex (V1) robustly respond to head movements, even in the absence of visual stimuli[6–8]. These responses depend on vestibular organs and dynamically track the time course of head movements, demonstrating specificity for aspects such as direction and velocity[7,8]. In contrast to our thorough understanding of the origin and processing of visual signals in V1, our understanding of head movement signals in this structure is still rudimentary. Is there a laminar organization in the representation of head movement signals in V1 as there is for visual information? Are head movement variables, such as direction and speed, computed in V1 or inherited from upstream structures? And, crucially, what are these upstream structures that relay head movement information to V1?

Here we use the mouse as a model system to determine the dynamics of V1 activity in response to head movement and reveal that the pulvinar nucleus of the thalamus, which receives axonal projections from the deep cerebellar nuclei (DCN), represents the main source of head movement signals to V1. We show that head movement variables, like direction and speed, are more accurately represented in the deep than the superficial layers of V1 and that these variables, rather than being computed *ex novo* in V1, are inherited from the pulvinar. The pulvinar, however, provides V1 with head movement signals that are biased toward contraversive movements (e.g. clockwise movements in left V1). Unexpectedly, we show that the contralateral visual cortex (VC) also provides V1 with head movement signals which, in contrast to the pulvinar, are stronger during ipsiversive head movements, and thus counterbalance the pulvinar bias. These results show that V1's rich representation of an animal's head movement variables results from the integration of inter- and intrahemispheric signals.

Results

Head Movement Encoding in V1

We recorded extracellular activity in the left V1 of head-fixed, awake mice in response to vestibular stimulation, delivered in the dark, by rotating the animal along the horizontal plane with a servo-controlled rotating table (Figure 1A, top). This protocol elicits responses in V1 that entirely depend on the vestibular organs[7,8]. Most V1 neurons (63%, 1490/2355 neurons, N = 37 mice) responded to clockwise (CW; i.e. contraversive relative to left V1: 49%, 1152/2355 neurons) and/or counterclockwise (CCW; i.e. ipsiversive relative to left V1: 47%, 1112/2355 neurons) rotations of the table, by either increasing or decreasing their firing rate (FR), as described previously (see Methods for class assignment criteria and statistical tests throughout).

Head movements trigger compensatory eye movements in the opposite direction via the vestibulo-ocular reflex (VOR). Since eye movements are known to modulate V1 neuronal activity[10–12], we tested whether V1 neurons can respond to head movements independently of eye movements. For this, we implemented a vestibular stimulation protocol that eliminates VOR, called VOR cancellation (see Methods). Here, instead of rotating the animal in the dark, we present a visual environment that rotates with the animal, thereby preventing compensatory eye movements (Figure S1). Even during VOR cancellation, 66% of V1 neurons responded to head movements (231/351 neurons; N = 5 mice; P = 0.18 compared to vestibular stimulation in the dark). Thus, the activity of V1 neurons is strongly modulated by head movements even in the absence of eye movements. All subsequent experiments were conducted in the dark.

V1 neurons responded to both CW and CCW head movement; however, we observed a stronger response to CW versus CCW rotations (|Z-scored FR|: 1.16±0.05 and 0.85±0.03, P = $4.5e^{-3}$). Furthermore, about a third of these neurons (35%, 834/2355 neurons) showed a significant direction preference (see Methods for class assignment criteria), as previously reported[7]. Among this population, neurons preferring CW rotations were slightly overrepresented (55%, 455/834 neurons prefer CW rotations, P = 0.0035). To investigate whether the preference for CW rotations in left V1 represents hemispheric specialization, we recorded from V1 neurons in the right hemisphere. We found that right V1 neurons showed a bias toward CCW head rotation. Specifically, the proportion of neurons preferring CW rotations in right V1 was significantly lower than in left V1 (45%, 48/106 neurons, P = 0.014), while the preference for CCW rotations mirrored the CW bias observed in left V1 (55%, 58/106 neurons, P = 0.4). These results reveal that in V1, neurons respond to head movements with a slight overrepresentation for contraversive rotations.

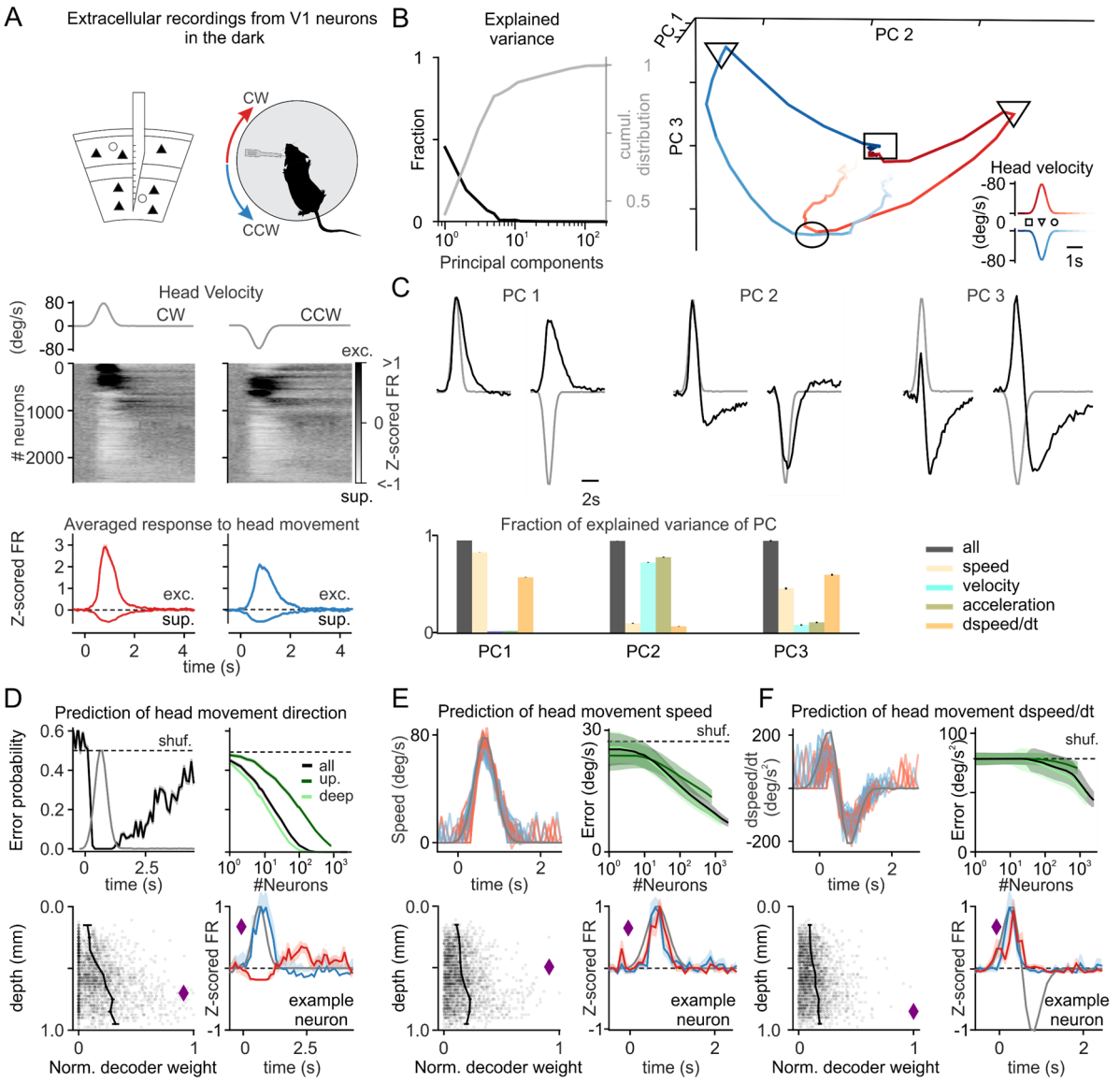

Figure 1. Head movement encoding in V1 in the absence of visual stimuli

(**A**) Experimental configuration (top). Extracellular linear probe in the left V1 of a head-fixed, awake mouse records the response to clockwise (CW) and counterclockwise (CCW) rotations of the table in the dark. Velocity profile (middle panel) and UMAP sorting of the responses (averaged Z-score of the firing rate (FR) across neurons. Average Z-scored FR of neurons significantly excited (exc.) or suppressed (sup.) by head movement in CW (red) and CCW (blue) direction.

(**B**) Principal component analysis of V1 population activity during head movement. Fraction of explained variance (black) and its cumulative distribution (gray) as a function of increasing principal component (PC) (left). Three-dimensional representation of the first three PCs showing a separation of CW (red) and CCW (blue) representation in V1 activity (right, time is color coded, and square, triangle and circle symbols indicate beginning, peak, and end of the rotation, respectively).

(**C**) Population dynamics along the first three PCs (black) superimposed on the velocity profile (gray) (top). Variance explained in each PC by models including speed, velocity, and their time derivative either all together (gray) or separately (color) (bottom).

(**D**) Representation of head movement direction in a trial: decoding error probability as a function of time (top left) and of number of neurons (top right, computed at peak velocity), decoder weight of single neurons and population average (bin = 100 μm) as a function of depth (bottom left), and example neuron (purple diamond) selected using highest decoder weight for head movement direction, at the peak and 2s after the peak velocity (bottom right).
(**E**) Instantaneous head angular speed representation: Prediction of head movement angular speed (top left), error as a function of number of neurons (top right, color indicates depth as in D), decoder weight of single neuron as a function of depth (bottom left), and example neuron (purple diamond) selected using highest decoder weight for head angular velocity decoding (bottom right).
(**F**) Analogous to E but for the time derivative of speed.
In panels A, B, and D-F, blue and red traces correspond to quantities measured during CCW and CW rotations, respectively.
Related to Figures S1 and S2

Despite the simplicity of the stimulus used, neurons showed substantial heterogeneity in their modulation profile with different amplitudes, kinetics, and sign of the modulation (Figure 1A, middle). To probe the structure of the population dynamics underlying this heterogeneous response, we performed principal component (PC) analysis. The first five PCs explained a substantial fraction of variance (Figure 1B, left; cumulative variance explained 0.89, variance explained by each PC≥0.05, see Methods).

To obtain an intuition of what this population dynamics might represent, we visualised activity along the first three PCs (Figure 1B, right). Prior to head movement onset, the population activity occupied a confined region of neural space. As the angular speed (the absolute value of angular velocity) of the head increased, two separate trajectories emerged, corresponding to CW and CCW head movements. Interestingly, the population dynamics observed with decreasing speed did not overlap with that of increasing speed, and this differential representation persisted for several seconds after the head movement ceased (3.7s, $P<0.05$, Wilcoxon rank-sum test, Figure. 1B,C). These observations suggest that V1 encoding of head movement information extends beyond instantaneous speed to include both the direction of movement and the history of previous movements.

To characterise which aspects of animal head movement were encoded in each PC, we fitted the corresponding dynamics through a linear combination of head movement-related variables, namely speed, velocity, (positive and negative velocities represented CW and CCW rotations, respectively) and their time derivatives. This model captured the dynamics along the five investigated PCs (Figure 1C, bottom; fraction of explained variance ≥0.72). We estimated the contribution of each head movement-related variable to V1 activity, by repeating the fitting procedure for each of them separately (Figure 1C, bottom). Along PC1, speed and its derivative explained 86% and 60% of the variance, respectively; along PC2, velocity and acceleration explained 75% and 80%; along PC3, speed and its derivative explained 46% and 61%.

Thus, the velocity and speed of head movements, as well as their time derivatives, are key factors in determining the dynamics of the activity of neuronal populations in V1.

To test if these variables could be reliably decoded on a trial-by-trial basis, we developed a decoding analysis. We first investigated the encoding of head movement direction (i.e. CW or CCW) by training a set of logistic regression models to predict head movement direction based on recorded neural activity in 100ms bins (Figure 1D, top left panel, see Method). Using the activity from all the recorded neurons (n = 2355), decoding error probability was at chance level prior to head movement onset and decreased below 0.05% in less than 300ms after movement initiation. Consistent with what was observed from population dynamics, accuracy remained above chance for 3.7s after movement offset. Accuracy rapidly increased with the number of neurons used and less than 600 randomly selected neurons were required to obtain more than 99.5% accuracy (Figure 1D, top right panel). The contribution of neurons to the decoder accuracy depended on their laminar location. Decoders based only on neurons in deeper layers (below 500μm from the pial surface) performed better than decoders based on neurons in superficial layers (above 500μm from the pial surface), with an equal number of neurons; accordingly, neurons in deeper layers had higher decoder weights (Figure 1D, bottom left panel). Furthermore, single neurons with high decoder weight were sufficient to predict head movement direction in a trial with an accuracy exceeding 99.5% (Figure S2D).

The speed of head movements could also be accurately predicted from V1 population activity (error=6.8±0.8 deg/s with 2355 neurons and neural activity binned in 100ms time windows; Figure 1E, top left). Again, neurons in deeper layers were more informative about speed (Figure 1E top right and bottom). Unlike what was observed for head movement direction, however, where neurons with high decoder weight could show differential responses between CCW and CW trials outlasting the head movement by several seconds, firing rates of neurons with high decoder weight for speed faithfully tracked instantaneous head speed; approximately 30 of these neurons were sufficient to obtain a decoding accuracy similar to that obtained with the whole recorded ensemble (11.9±2.1 deg/s, Figure S2D). The derivative of speed (Figure 1F), velocity (Figure S2B) and acceleration (Figure S2C) were decoded with analogous performance. Importantly, the decoded representation did not depend on the specific head movement profile experienced by the animal. First, a decoder trained on the rising phase of the head velocity profile generalized to the decaying phase of this profile with the same velocities (Figure S2A). Second, a decoder trained on a given profile generalized to head movements with same peak velocity but different acceleration (Figure S2E).

Taken together, these results show that mouse V1, and especially its deeper layers, encodes a rich representation of head movement that can be accessed to simultaneously decode present and past movements with high precision.

Pulvinar origin of head movement signals to V1

What could be the sources of the head movement signals that reach V1? To identify potential upstream candidate areas, we injected an anterograde transsynaptic tracer in the DCN, one of the main sources of vestibular signals to the brain. Injection of AAV2/1-hSyn-Cre in the DCN of a tdTomato reporter mouse labelled neurons throughout the thalamus, in agreement with previous work[13,14]. Among visual areas, only the pulvinar thalamus receives direct DCN projections (Figure 2A). In contrast, DCN injections labelled very few neurons in the dLGN, the other main thalamic relay to visual cortex, nor did they label neurons in V1 (pulvinar: 896.5±97.8 per mm^3; dLGN: 27.8±5.7 per mm^3, P = $6.6e^{-17}$; no labelled neurons in V1; n = 123 slices, N = 8 mice), consistent with the lack of direct projection from DCN to the cortex[13–15]. We confirmed the specificity of the DCN projections to the pulvinar using a retrograde tracer. Injection of retrograde AAV-Cre in the pulvinar of tdTomato reporter mice labelled many more neurons in the DCN than in the other main source of vestibular signal in the brain – the vestibular nuclei (DCN: 682.4±82.7mm^3; VN: 94.54±27.0 mm^3, P = $2.7e^{-11}$, n = 40 slices, N = 3 mice, Figure S3A-C). Thus, pulvinar neurons receive direct projections from the DCN, making this thalamic nucleus a potential node for vestibular signals on their way to V1.

If the pulvinar is a source of head movement signals to the visual cortex, it must respond to head movements. Thus, we recorded neuronal activity from the left pulvinar of head-fixed, awake mice in response to vestibular stimulation delivered in the dark by rotating the animal along the horizontal plane (Figure S3D), as we did for V1 recordings (see above). Similar to V1, the firing rate of most pulvinar neurons (73%; 258/355 neurons; n = 11 mice) was modulated by CW (58%; 207/355 neurons) and/or CCW (51%; 182/355 neurons) rotations of the table and a large fraction of these neurons (45%; 160/355 neurons) showed a significant direction preference (Figure 2B). Furthermore, the response of left pulvinar was also biased towards CW head movements (average Z-scored FR: CW, 1.36±0.10; CCW, 1.04±0.08; P = $3.72e^{-3}$). In fact, the pulvinar showed a larger fraction of neurons preferring CW rotations than V1 (100/160, 62% observed in the pulvinar versus 455/834, 54% observed in V1, P = 0.037). Finally, principal component analysis of pulvinar activity during head movement showed a remarkable similarity with that observed in V1 (Figure 2C). Specifically, the activity along the first three PCs (Figure 2C, top right and bottom) closely matched those observed in V1 and the first five PCs were explained by head movement-related variables in an analogous way to V1 (Figure 2C, bottom right). The similarity between head movement representation properties in the pulvinar and V1 were equally striking when quantified with a decoding analysis. Decoding performances of trial head movement direction as a function of time (Figure 2D), as well as of speed (Figure 2E), velocity (Figure S3E), and their time derivatives (derivative of speed: Figure 2F; acceleration: Figure 3F), closely resemble what we observed in V1.

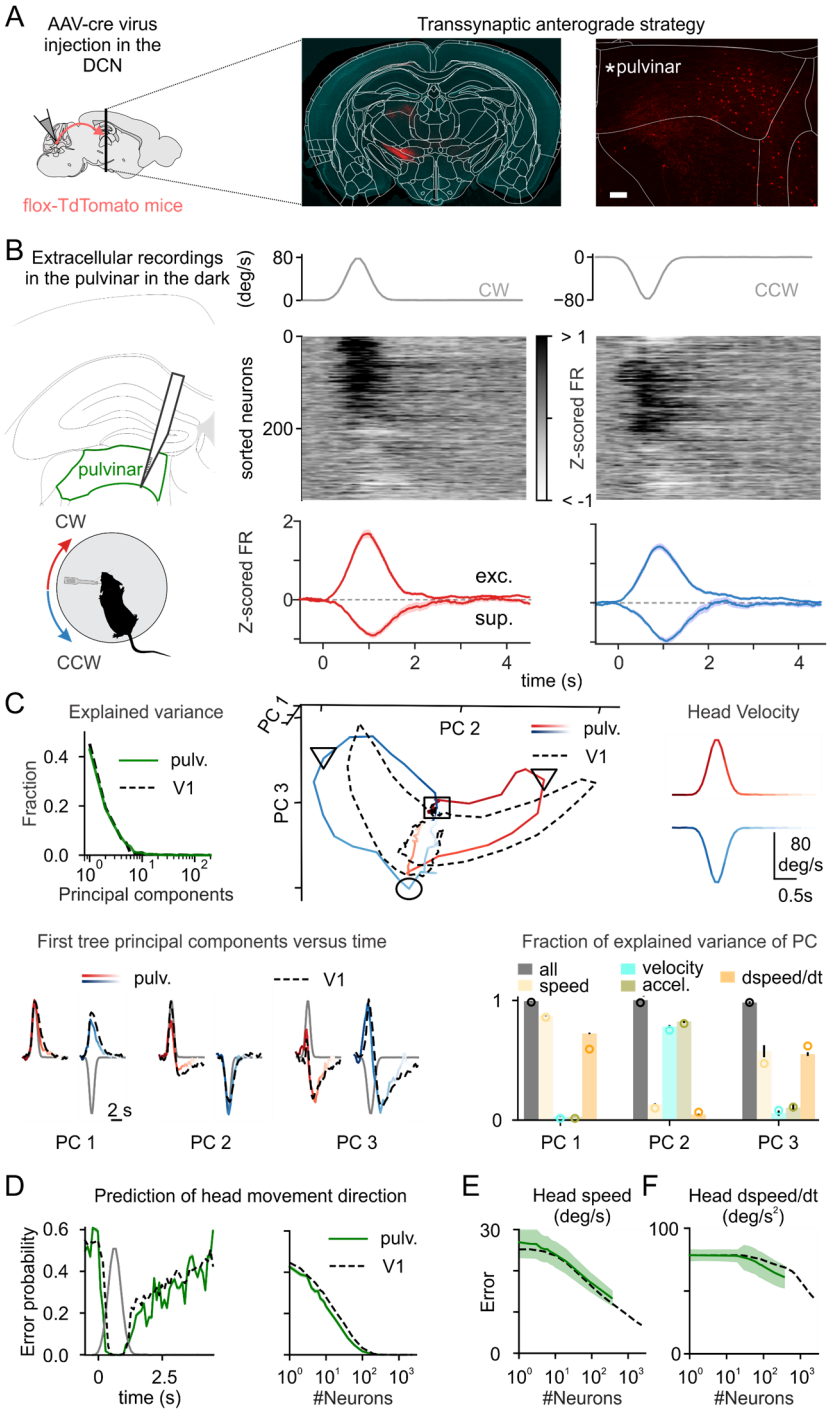

Figure 2. The pulvinar thalamus receives projection from the DCN and shows a head movement representation similar to V1

(A) Experimental strategy (top). Injection of Cre dependent transsynaptic anterograde virus (AAV2.1 hSyn-cre) in the deep cerebellar nuclei (DCN) in a flex-tdTomato reporter line; this approach labels the projections of the DCN and the post-synaptic cells in red (see Methods). Scale bar = 100 µm.

(B) Experimental configuration (top). Extracellular linear probe in the left pulvinar thalamus of a head-fixed, awake mouse records the response to clockwise (CW, red) and counterclockwise (CCW, blue) rotations of the table in the dark. Velocity profile (top, dark traces), UMAP sorting of the averaged Z-score of the firing rate (Z-scored FR) responses

across neurons (middle), and Z-scored FR of pulvinar neurons that significantly respond to CW (left) and CCW (right) head movement.
(C) Comparison of principal component analysis in pulvinar and V1. Black dashed lines correspond to quantities measured in V1, as described in Figure 1B and green lines correspond to pulvinar recording (top left). Three-dimensional representation of the first three PCs for V1 (dashed lines) and the pulvinar activity (time is color coded: CW (red) and CCW (blue) rotations; square, triangle and circle symbols indicate beginning, peak, and end of the rotation, respectively). Variance explained in each PC by models including speed, velocity, and their time derivative either all together (gray) or separately (color) (bottom). Circles are the fraction of explained variance in V1 (see Figure 1C).
(D) Decoding error probability of head movement direction in a trial as a function of time (left) and of number of neurons (right, computed at peak velocity), in pulvinar (green) and V1 (black).
(E) Decoding error of head movement angular speed as a function of number of neurons in pulvinar (green) and V1 (black).
(F) As in E but for head angular derivative of speed in time.
For (C-F): Head movement representation is analogous to that observed in V1.
Related to Figure S3.

Taken together, these results show that head movements modulate the activity of a large fraction of pulvinar neurons to generate a rich representation that matches the one observed in V1, albeit with a stronger bias towards contraversive movements. Thus, the pulvinar is a potential source of vestibular signals upstream of V1.

To determine whether the pulvinar contributes to the representation of head movements in V1, we pharmacologically silenced this thalamic area while simultaneously recording V1 activity in response to vestibular stimulation. The stereotactic injection of the GABAergic agonist muscimol into the left pulvinar resulted in a slight decrease in the basal activity of V1 neurons (control average FR = 3.77±0.29 Hz, pulvinar silencing FR = 3.44±0.26 Hz, P = 0.001). Yet, it caused a strong reduction of their response to head movements (CW: 72±5% decrease of Z-scored FR, P = $1.5e^{-8}$; CCW: 54±6% decrease of Z-scored FR, P = $1.7e^{-5}$; Figure 3). This effect was more pronounced for CW rotations (CW versus CCW: P = 0.006, Figure 3), consistent with the biased representation of CW head movements in the pulvinar (see above).

Taken together, these results indicate that the pulvinar is a main source of vestibular signal to V1 with a bias toward contraversive head movements.

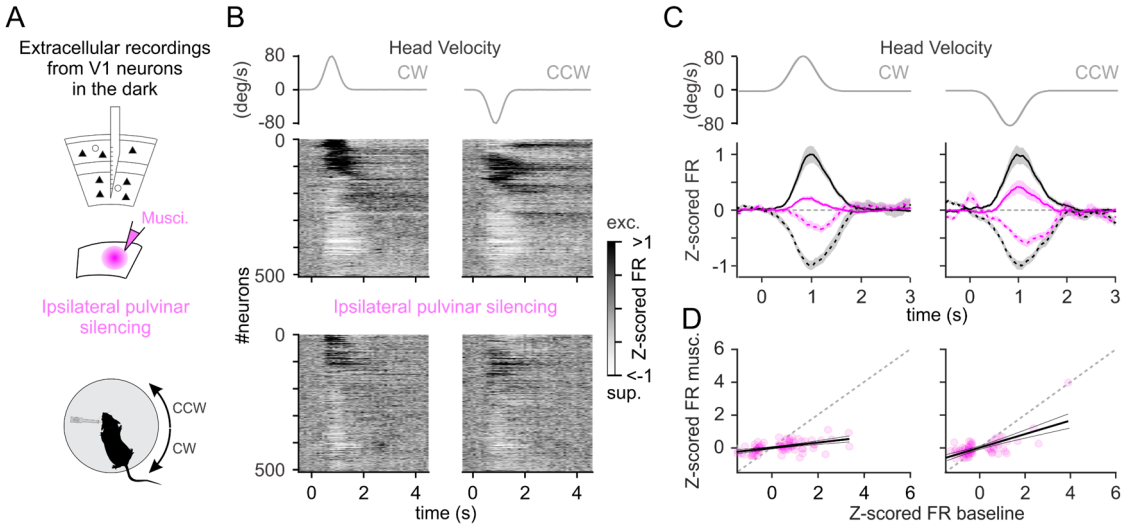

Figure 3. The ipsilateral pulvinar is a source of vestibular signal to V1 biased toward CW head movement.

(A) Experimental configuration. Extracellular linear probe in the left V1 of a head-fixed, awake mouse records the response to clockwise (CW) and counterclockwise (CCW) rotations of the table in the dark before and after pulvinar silencing by injecting muscimol-BODIPY.

(B) Velocity profile (top) and UMAP sorting of the averaged Z-score of the firing rate (Z-scored FR) of V1 neurons in response to head movements before (middle) and after (bottom) pulvinar silencing.

(C) Peak normalized Z-scored FR of V1 neurons during CW (left panels) and CCW (right panels) head movements before (dark traces) and after (magenta traces) ipsilateral pulvinar silencing (top). Note that for C and D, only neurons significantly modulated during head movements under control condition contribute to each average depending on whether they were excited (solid lines) or suppressed (dashed lines) by the rotation. All traces are normalized by the peak of the Z-scored FR under control condition. The gray (top), black and magenta (bottom) traces represent the velocity profiles of the table, the control condition and the ipsilateral pulvinar silencing, respectively.

(D) The peak Z-scored FR during CW (left) and CCW (right) head movement in control condition (x-axis) versus pulvinar silencing (y-axis). Magenta circles represent neurons that significantly respond to head movement during baseline condition, respectively.

Contralateral visual cortex contribution of head movement signals to V1

The fact that silencing the left pulvinar reduces responses in left V1 to CW more than to CCW rotations suggests that left V1 receives CCW head movement signals from an additional source. Because responses in right V1 are biased towards CCW rotations, and V1 hemispheres are connected via transcallosal projections[16,17], we tested the potential contribution for right V1 to CCW head movement signals in left V1.

For this, we optogenetically silenced the right visual cortex while recording from left V1 (Figure 4A). Silencing was achieved by photo-activating inhibitory neurons expressing Channelrhodopsin2 (ChR2; VGat-ChR2-EYFP mouse line) with an LED

placed on top of the right visual cortex, as described previously[18–20]. Silencing trials were alternated with control ones without any LED illumination. We prevented LED evoked visual responses (i.e. LED light hitting the retina) to contaminate our V1 recordings by performing experiments in mice previously blinded by intraocular TTX injections in both eyes (see Methods). LED illumination led to a slight decrease in the average basal activity of left V1 neurons (baseline average FR = 2.78±0.20Hz, contralateral VC silencing FR = 2.70±0.19Hz, P = 1.8e^{-10}; 23% (95/408) of the neurons are suppressed and 19% (75/408) excited). Strikingly, silencing the right visual cortex selectively reduced responses to CCW head rotations in left V1 (33.2±5.7% decrease of Z-scored FR) leaving responses to CW rotations unaffected (11.6±5.7% decrease of Z-scored FR; CCW versus baseline: P = 8.0e^{-10}; CW versus baseline: P = 0.83, CW versus CCW: P = 0.0001; Figure 4A-E). Thus, the right visual cortex is a source of CCW head movement signals to left V1.

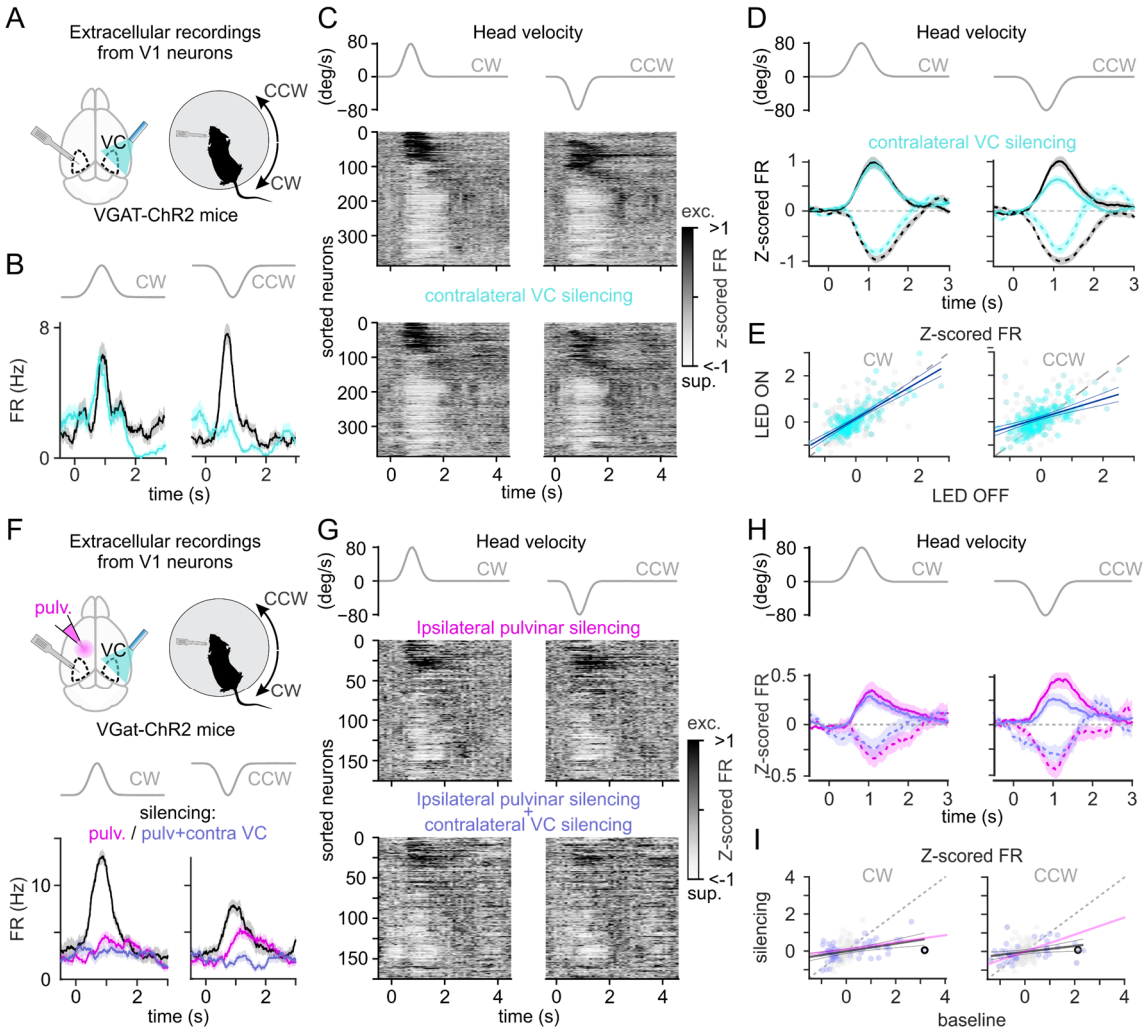

Figure 4. The ipsilateral pulvinar and the contralateral visual cortex are sources of vestibular signal to V1

(**A**) Experimental configuration (top). Extracellular linear probe in the left V1 of a head-fixed, awake mouse records the response to clockwise (CW) and counterclockwise (CCW) rotations of the table while silencing the contralateral visual cortex (VC).
(**B**) Effect of silencing contralateral VC on an example neuron recorded in left V1. Z-score of the firing rate (Z-scored FR) of a V1 neuron during CW (left) and CCW (right) head movements before (dark traces) and during contralateral VC silencing (cyan traces). The gray trace is the velocity profile.
(**C**) Velocity profile (top) and UMAP sorting of the averaged Z-scored FR of V1 neurons in responses to CW (left) and CCW (right) head movements before (middle), and during contralateral VC silencing (bottom).
(**D**) Peak normalized Z-scored FR of V1 neurons during CW (left) and CCW (right) head movements before (dark traces) and during contralateral VC silencing (cyan traces). Only neurons significantly modulated by head movements in the control baseline contribute to each average depending on whether they were excited (solid lines) or suppressed (dashed lines) by head rotation. All traces are normalized by the peak Z-scored FR observed in control condition. The gray trace is the velocity profile.
(**E**) Relation between Z-scored FR in control versus contralateral VC silencing conditions. Same neurons as in D.
(**F**) Experimental configuration (top). Extracellular linear probe in the left V1 of a head-fixed, awake mouse records the response to clockwise (CW) and counterclockwise (CCW) rotations of the table performing periodic contralateral VC silencing before and after ipsilateral pulvinar silencing. Effect of silencing contralateral VC and ipsilateral pulvinar on an example neuron (bottom). Z-scored FR of a V1 neuron during CW (left) and CCW (right) head movements before (dark traces), during ipsilateral pulvinar silencing (magenta traces), and during simultaneous ipsilateral pulvinar and contralateral VC silencing (purple traces). The gray trace is the velocity profile.
(**G**) Velocity profile (top) and UMAP sorting of the averaged Z-scored FR of V1 neurons in responses to CW (left) and CCW (right) head movements after ipsilateral pulvinar silencing only (top) and with both ipsilateral pulvinar and contralateral VC silencing (bottom).
(**H**) All traces are normalized by the peak Z-scored FR observed under control condition. Peak normalized Z-scored FR of V1 neurons during CW (left) and CCW (right) head movements after ipsilateral pulvinar silencing (magenta traces) and during contralateral VC and pulvinar silencing (purple trace). Only neurons significantly modulated during head movements in the control condition contribute to each average depending on whether they were excited (solid line) or suppressed (dashed line) by the rotation. The gray trace is the velocity profile. Note that the control condition is not represented.
(**I**) Relation between Z-scored FR in control versus simultaneous contralateral VC silencing and ipsilateral pulvinar silencing conditions. Bold circles report the example neuron in F.

If the ipsilateral pulvinar and the contralateral cortex independently contribute to head movement responses in V1, CCW responses remaining in left V1 after pulvinar silencing should be further reduced with the silencing of the right visual cortex. We tested this possibility by combining the pharmacological silencing of the pulvinar with the optogenetic silencing of the visual cortex. Consistent with this hypothesis, optogenetic silencing of the right visual cortex performed following the

pharmacological silencing of the left pulvinar selectively reduced the remaining responses to CCW rotations in left V1 (Figure 4F-H).

Taken together, these results indicate that the ipsilateral pulvinar is the main contributor to V1 responses to head movements, with a bias towards contraversive rotations and that the contralateral visual cortex contributes to response to ipsiversive rotations. Thus, the ipsilateral pulvinar and, to a lesser extent, the contralateral visual cortex are two independent sources of vestibular signal to V1, each preferentially contributing to responses in opposite directions along the horizontal plane.

Discussion

Primary sensory areas in the cerebral cortex process modality specific sensory information originating from peripheral receptors, such as those for vision, hearing, and touch. Some recent discoveries, however, have challenged this strict, modality specific view of primary sensory cortical areas[7,11,21–24]. A striking example is that V1 responds robustly to head rotations via vestibular organ activation[7,8], even in complete darkness. A clear example is the observation that V1 robustly responds to head rotations through the activation of vestibular organs[7,8] even in the complete absence of visual stimuli. Thus, V1 is a primary sensory cortical area that not only receives ascending input from the eye and responds to visual stimuli, but also responds to vestibular stimuli. This observation has opened several fundamental questions, relative to the anatomical pathways taken by these vestibular signals to reach V1, the nature of the representation of head movement variables in V1 and the extent to which the representation of these variables is inherited from upstream structures. Here, we demonstrate that V1 accurately encodes head movement variables (direction, speed, velocity, and their time derivatives) especially in deeper layers, and that it receives head movement signals through two main pathways: the ipsilateral pulvinar nucleus of the thalamus and the contralateral visual cortex. The ipsilateral pulvinar provides the predominant head movement signal, exhibiting a bias toward contraversive rotations (e.g., clockwise rotations relative to left V1). In contrast, the contralateral visual cortex contributes head movement signals during ipsiversive rotations. Importantly, we found that head movement variables in V1 are already represented in the pulvinar, suggesting that V1 inherits these variables rather than computing them *ex novo*. These results demonstrate that the integration of intra- and interhemispheric signals endows V1 with a rich and accurate representation of head movements.

Sensory stimuli often trigger behavioral responses which, in turn, can lead to a cortex-wide modulation of neuronal activity. Consequently, some activity in primary cortical areas in response to stimuli of distinct modalities may be erroneously interpreted as multimodal responses. For example, a substantial portion of V1 neurons' response to auditory stimuli can be explained by facial movements triggered by the sound, and are thus not true auditory V1 responses[24,25]. In our experiments, head movement also triggered a behavioral response, namely compensatory eye movements through the activation of the VOR[10]. Given that the kinetics and amplitudes of the VOR are tightly linked to the kinetics and amplitude of head movements, V1 responses to head movement could, in theory, be explained by eye rather than head movements. This possibility would, furthermore, be consistent with the fact that the VOR, like the response of V1 to head movement, depends on the vestibular organ. To address this possibility, we used a well-established protocol to eliminate eye movements during head movement, called VOR cancellation[26]. Using this protocol, we still recorded strong responses of V1 neurons to head movement, demonstrating that these responses arise from head movement itself rather than from concurrent compensatory eye movements.

We show that silencing the pulvinar nucleus of the thalamus strongly reduces head movement signals in V1. Together with its DCN inputs and head movement signals that closely match V1's representation, the pulvinar serves as a key node for head movement processing upstream of V1. How do head movement signals in the pulvinar reach V1? The pulvinar sends direct axonal projections to V1. However, the pulvinar also projects to higher visual areas and to the retrosplenial cortex (RSC)[27–30] and these areas not only respond to head movement[6,8,9] but also project to V1[8,31]. Thus, V1 could receive head movement signals directly through the pulvinar, and/or indirectly via higher visual areas or the RSC. While direct projections imply a fundamental role for movement cues in early visual processing, indirect projections could support the integration of these signals with more abstract representation of visual stimuli[32].

The thalamus receives the majority of its vestibular input from the contralateral vestibular and cerebellar nuclei[13,14] and these nuclei are primarily biased towards ipsiversive movements. Consistent with this organization, we observed a contraversive movement bias in the pulvinar (i.e., clockwise for the left pulvinar). However, this contraversive bias of the pulvinar almost disappears in V1. We discovered that this rebalancing of motion specificity is due to input from the contralateral visual cortex. While the cortico-callosal projections in the binocular V1 have been well characterized[33], their role in monocular V1 is still unclear[17,18]. Here, we show that this interhemispheric communication to monocular V1 provides a head movement signal with a direction preference bias opposite to that obtained from the ipsilateral pulvinar. Whether this rebalancing is critical for a complete (ipsi- and contralateral) picture of motion, or if the segregation and recombining of motion signals serves a specific computational purpose remains to be seen.

Several pathways connect the vestibular system to the primate's thalamus[34], and accordingly, the pulvinar of these animals responds to various vestibular stimulation[35]. Furthermore, the pulvinar receives projections from motor areas, including the motor cortex and deep cerebellar nuclei[13,14,36], and projects broadly across the visual cortex, conveying not only visual information but also other non-visual inputs to V1[11,29]. Interestingly, inactivating the pulvinar abolishes the saccadic modulation observed in V1 neurons[11], highlighting the pulvinar's role in integrating both visual and non-visual information. Our results demonstrate that, in mice, the pulvinar serves as the primary source of head movement signals to V1. The convergence of head and eye movement signals with visual information in V1 through the pulvinar suggests a fundamental mechanism for maintaining stable perception during active behavior. Indeed, the pulvinar has recently emerged as critical for distinguishing self-generated from external visual motion[37], and its role in predictive coding[38] may reflect a broader strategy where the brain uses movement-related signals to anticipate sensory consequences. Future work will need to reveal how the pulvinar's diverse functions arise from its unique position between motor and sensory

systems, and how this integration shapes our perception of a stable visual world during self-motion.

In summary, the intra- and interhemispheric vestibular signals to V1 described here may impact cortical visual processing by providing a head movement context to incoming visual inputs. Understanding the origin and processing of these signals could provide critical insights into how the early visual system integrates visual input with contextual information related to motion, enhancing our understanding of sensory processing during action.

EXPERIMENTAL MODEL AND SUBJECT DETAILS

Mice

All experimental procedures were conducted in accordance with the regulations of the Institutional Animal Care and Use Committee (IACUC, AN179056) of the University of California, San Francisco.

All mice were housed on a reversed cycle (light/dark cycle 12/12 h) with free access to food. Data were collected from male or female C57BL/6J mice or from heterozygous mice kept on a C57BL/6J background with the following genotype: VGat–ChR2–EYFP (Jackson Labs #014548). V1 recordings in darkness included 1,502 units from 30 C57BL/6J mice, obtained from our previous study under identical experimental conditions[7]. At the start of the experiments, all mice were between 2 and 7 months old.

METHOD DETAILS

Viruses

The following adeno-associated viruses (AAV) were used: AAV1-hSyn-Cre-WPRE-hGH (final titer: 1.8×10^{13} genome copies/ml, Univ. of Pennsylvania Viral Vector Core) and AAV1-retro-hSyn-Cre-eBFP (final titer: 5×10^{12} genome copies/ml, Univ. of Pennsylvania Viral Vector Core).

Surgical procedures

Viral Injections

Mice were anesthetized with 2% isoflurane and placed in a stereotactic apparatus (Kopf). Core body temperature was monitored with a rectal probe and maintained constant at 37°C with a heating pad (FHC). A thin layer of lubricant ointment (Rugby Laboratories) was applied to the eye, the head was shaved and disinfected with povidone iodine, and 2% lidocaine solution was administered subcutaneously at the incision site. A craniotomy (approx. 300 µm in diameter) was performed with a micro-burr (Gesswein) mounted on a dental drill (Foredom). Viral suspensions were loaded in bevelled glass capillaries (tip diameter: 15-30 µm) and injected with a micropump

(UMP-3, WPI) at a rate of 30-40 nl/min into the parenchyma. The coordinates of the injection sites and the volumes of the injected viral suspension are detailed below. The pipette was removed from the brain 15 min after the completion of the injection, the head plate was attached just after the virus injection, and 0.1 mg/kg buprenorphine was administered subcutaneously as a postoperative analgesic. For anterograde transsynaptic strategy[39], the virus was injected in the right DCN (AP:-6.1mm,ML:2.0mm,depth:2.25mm). For retrograde strategy in the pulvinar, the virus was injected in the left rostro-medial pulvinar (AP:-1.9mm,ML:1mm,depth:2.4mm)

Head Plate Implantation for Head-fixed Recordings

Mice were implanted with a T-shaped head-bar at least 2.5 weeks before the day of the recording. Mice were anesthetized with 2% isoflurane, the scalp was removed, the skull was disinfected with alcohol and povidone iodine, and scored with bone scraper. The edge of the skin was glued to the skull and the metal head-bar was sterilized and mounted using dental cement (Ortho-Jet powder; Lang Dental) mixed with black paint (iron oxide), or Relyx Unicem2 automix (3M ESPE). The head-bar was stereotactically mounted with the help of an inclinometer (Digi-Key electronics 551-1002-1-ND). The inclinometer allowed us to adjust the angle of the head bar in relation to the sagittal and medio-lateral axes of the head. Following the bar implantation, black dental cement was used to build a recording well surrounding the recording site. The surface of the skull above the left visual cortex was not covered with dental cement but was coated with a thin layer of transparent cyanoacrylate glue. Mice were injected subcutaneously with 0.1 mg/kg buprenorphine and checked daily after the head-bar surgery. For at least 4 days before recording, mice were habituated to head fixation within the recording setup.

Craniotomy for Electrophysiological Recordings

On the day before recording, mice were anesthetized with 2% isoflurane and the skull above the recording sites was drilled off. The dura was not removed, and the exposed brain was kept moist with artificial cerebrospinal fluid (ACSF; 140mM NaCl, 5mM KCl, 10mM D-glucose, 10mM HEPES, 2mM CaCl2, 2mM MgSO4, pH 7.4). V1 recordings were performed at approximately 2.6 mm lateral to the sagittal suture and 0.6 mm anterior to the lambdoid suture.

Electrophysiology

Extracellular recordings were performed using the following silicon probes Neuronexus: A1x32-5mm-25-177-A32; A1x32-Edge5mm-20-177-A32; A2x32-5mm-

25-177-A64, 1x64-Poly2-6mm-23 s-160 or Cambridge Neurotech: ASSY-77 H2 (Acute 64 channel H2 probe, 2 shanks @250um, 8mm length), ASSY-77 H5 (Acute 64 channel H5 probe, 1 shank, 9 mm length). The recording electrodes were controlled with Luigs & Neumann micromanipulators and stained with DiI or DiO lipophilic dyes (Thermo Fisher) for post hoc identification of the electrode track. We recorded the signals at 30 kHz using an INTAN system (RHD2000 USB Interface Board, INTAN Technologies).

Head-fixed Rotations

To control the velocity and amplitude of head movements, we fixed the head of awake mice in the center of a servo-controlled platform enabling the rotation of the animal along the horizontal plane (50 degrees rotation; 80deg/s peak velocity, see Figure 1A; unless stated otherwise). Mice were head-fixed, their bodies restrained in a tube, and we pseudo-randomly alternated clockwise (CW) with counterclockwise (CCW) rotations. The platform was attached to a gearbox 15:1 (VTR010-015-RM-71 VTR, Thomson) that increased the torque of a servo motor (AKM53L-ANC2C-00 KEC0432 AC Servomotor 1.83kW, Kollmorgen). The motor was tuned using a servo drive (AKDB013206-NBAN-0000 servo drive, Kollmorgen) and controlled in velocity mode using analog waveforms computed in Labview.

Monitoring eye movements by video-oculography

The movement of the right eye was monitored through a high-speed infrared (IR) camera (Imperx Bobcat, B0620). The camera captured the reflection of the eye on an IR mirror (transparent to visible light, Edmund Optics #64–471) under the control of custom Labview software and a frame grabber (National Instrument PCIe-1427). The pupil was identified online or post hoc by thresholding pixel values and its profile was fitted with an ellipse to determine the center. The eye position was measured by computing the distance between the pupil center and the corneal reflection of a reference IR LED placed along the optical axis of the camera. To calibrate the measurement of the eye position, the camera and the reference IR LED were moved along a circumference centered on the image of the eye by ± 10 degrees[40].

Vestibulo-ocular reflex paradigms

To assess vestibulo-ocular reflex (VOR) compensation and cancellation, well-habituated mice were head-fixed on a rotating platform surrounded by a visual virtual stimulus drum. We presented visual stimuli (0.1cpd) moving synchronously with the turntable (20 deg peak velocity, 1.8s, 15deg) during VOR cancellation and static during

VOR compensation trials. Eye movements were tracked as described above. During VOR cancellation trials, the platform and visual drum were rotated using a gaussian velocity waveform in the same direction and at matching velocities. This condition required mice to suppress their VOR to maintain a stable gaze on the moving visual stimulus. Eye position data were analyzed offline using custom MATLAB scripts to calculate gain (ratio of eye and head velocity). VOR cancellation performance was quantified as the absence of reflexive eye movement, while expecting a reflexive eye movement in the opposite direction during VOR compensation. Rapid eye movements were excluded from our analysis.

Pharmacology

Intraocular injection of tetrodotoxin (TTX; 40 µM) was performed 2 hours prior to recording, under isoflurane anesthesia. A typical procedure lasted less than five minutes. TTX was injected in both eyes for all the experiments performed on VGat-ChR2-EYFP mice. Immediately prior to the injection, a drop of proparacaine hydrochloride ophthalmic solution was applied to the eye as a local anaesthetic (Bausch + Lomb, 0.5%). TTX solution was injected intravitreally using a bevelled glass micropipette (tip diameter ~50 µm) on a micro injector (Nanoject II, Drummond) mounted on a manual manipulator. 1 µl was injected in each eye, at the speed of 46 nl/s. The animals were head-fixed for recording following a 2-hour recovery period in their home cage.

Silencing of the pulvinar was performed by injecting 30-40 nl of 5 mM muscimol-BODIPY at the speed of 80-150 nl/min, using a bevelled glass pipette (tip diameter ~ 20-40 µm) on a micro injector UMP3 with a Micro4 controller (World Precision Instruments). The injector was mounted on a micromanipulator (Luigs & Neumann) for stereotactic injection. After the recording, brains were fixed in 4% PFA in PBS overnight at 4°C for histological analysis of BODIPY on the next day.

To verify the absence of visual responses following intraocular TTX injection, we used a full-field luminance change from 0 $cd.m^{-2}$ to 100 $cd.m^{-2}$ lasting 1s.

Optogenetic silencing of contralateral visual cortex

Cortical silencing was achieved by expressing channelrhodopsin-2 (ChR2) in inhibitory neurons, a technique previously validated[19–21,37]. We utilized the VGat–ChR2–EYFP mouse line for optogenetic silencing of the contralateral visual cortex. For photostimulation of ChR2-expressing cortical inhibitory neurons, we positioned a 470-nm blue fiber-coupled LED (1 mm diameter, Doric Lenses) approximately 5–10 mm above a thinned skull area on the right hemisphere of the visual cortex. To limit illumination to the tissue under the cranial window, we covered adjacent areas with

black dental cement. To prevent inadvertent retinal stimulation from blue light and conserve the pitch-dark condition, we performed bilateral eye injections of TTX to induce temporary blindness. The LED fiber delivered a total light power of 8-15 mW. We alternated trials between head rotation alone and head rotation combined with LED illumination. The LED was activated for 4s, centered on the peak velocity of the head rotation.

Histology

For anatomical analysis, mice were transcardially perfused with phosphate buffered saline (PBS) and then with 4% paraformaldehyde (PFA) in PBS. Brains were extracted from the skulls, post-fixed in 4% PFA overnight at 4C, and subsequently cut with a vibratome to 80-100 μm thick sequential coronal sections. Slices were collected and mounted in ProLong Gold (Life Technologies) or Vectashield mounting medium containing DAPI (Vector Laboratories H1500). Bright-field and fluorescence images were acquired using an Olympus MVX10 MacroView microscope. For quantifying the number of somas in the visual thalamus, deep cerebellar nuclei, and vestibular nuclei (see sections: *Viruses* and *Viral Injections*), neuronal density was counted for each brain slice and then averaged. Ipsilateral projections for both DCN and pulvinar tracing experiments were negligible and not considered. The Paxinos brain atlas was used as a reference to delineate these regions.

QUANTIFICATION AND STATISTICAL ANALYSIS

Data Analysis

Unit isolation

Automated spike sorting was carried out using KiloSort and KiloSort2 (https://github.com/cortex-lab/Kilosort) by manual curation of the units using Phy and Phy2 (https://github.com/cortex-lab/phy). Single units were identified, and all the following analysis was carried out via MATLAB (MathWorks), but for principal component and decoding analysis (Python 3). We excluded units where more than 1-2% of spikes occurred within the refractory period.

Class assignment criteria

To classify the units that are significantly modulated by head movement, we compared its neuronal activity before and during head rotation. The baseline spike rate was calculated on individual trials by averaging the spike rate over a window of 580 or 1000ms recorded when the platform was stationary before the rotation. The spike rate in response to the rotation of the platform was calculated on the same trials by averaging the spike rate over a window of 580ms centered around the peak of the rotation velocity profile. Wilcoxon signed-rank tests were then applied to determine if a unit was significantly modulated ($P < 0.05$) by the rotation of the platform. Directional preference of individual unit was quantified by comparing their firing rate in response to CW and CCW rotations. For each recorded unit, we computed the mean firing rate within a 580ms temporal window centered on the peak angular velocity of platform rotation. To establish directional tuning, firing rates during CW and CCW rotations were compared using non-parametric Wilcoxon signed-rank tests, with statistical significance set at $P < 0.05$. This analysis enabled identification of neurons exhibiting preferential responses to specific rotation directions. To compare the Z-score of the firing rate collected from 2 populations of mice, we performed Wilcoxon rank sum tests. When reporting averaged absolute Z-score of the firing rate, only neurons significantly modulated by head movement in baseline condition were included. Wilcoxon signed rank tests were performed to compare values obtained in the same recording (i.e., comparing before and during thalamus or contralateral visual cortex silencing).

Cortical depth estimation

Cortical depth from pia estimated by using electrophysiological landmarks across layers as described previously[7,41]. Briefly, the Multi-unit (MUA) spectral power (500 Hz to 5 kHz) distribution along the probe track allowed us to locate layer 5a. This approach allowed us to normalize the cortical depth from the pia across mice.

Statistics

Statistical analyses were done using MATLAB and Python 3. No statistical tests were used to predetermine sample size, but our sample sizes are similar to those generally employed in the field. All data are presented as mean ± standard error of the mean (SEM), unless otherwise noted. The stated P values are the results of the non-parametric Wilcoxon rank sum test to compare values between different mice or recordings, and the non-parametric Wilcoxon signed rank test to compare values from the same recording in different experimental conditions. The difference of fraction of neurons modulated across brain areas was accessed using the bootstrap hypothesis test. Specifically, we resampled neurons with replacement from our dataset of Z-score

of the firing rate responses to clockwise (CW) and counterclockwise (CCW) rotations (N = 10000 iterations). For each bootstrap sample, we computed response amplitudes and firing rate changes, then fitted Gaussian functions to the cumulative distribution functions to calculate p-values, determining the statistical significance of observed differences. For the anatomical tracing analysis, the non-parametric Wilcoxon rank test was employed to compare the values between slices from the VN and the DCN, as well as between slices from the dLGN and the pulvinar. Experiments and analyses were not blinded.

Cross validated cell sorting and principal component analysis

For recordings in V1 and pulvinar in control conditions, trials were divided in two equally populated sets (called in what follows training and test sets); a trial averaged response was computed for each neuron separately in the two sets. Neurons were ordered using the UMAP algorithm applied to the training set of the control conditions[42]. This ordering was then applied to the test set to obtain the UMAP plots shown throughout the text.

Cross-validated principal component analysis activity[22] was used to estimate the fraction of variance explained by each principal component. In brief, we computed the trial averaged response of neurons in each realization of the training and test sets. The training set was used to derive the principal components, while the test set was used to measure the variance explained in each component. The procedure was repeated ten times with different random realizations of the training and test sets; means and standard errors over realizations are shown in Figure 1B, 1C, and 2C. As shown by Stringer et al.[22], this method measures the reliable variance of stimulus-related dimensions, excluding trial-to-trial variability from unrelated cognitive and/or behavioural variables or noise. For recordings in V1 and the pulvinar, the first 3 (pulvinar: 5) PCs accounted for 76% and 74% (pulvinar: 87% and 85%) of the variance, respectively.

Relationship between principal components and movement

To quantify the relation between movement and neural activity along each principal component (PC), we defined a predictor y(t) given by

$$y(t) = \sum_{i=1}^{4} \quad a_i \int_{-\infty}^{t} \quad dt' \, e^{(t'-t)/\tau_i} x_i(t')/\tau_i,$$

where the index i runs over the movement related variables investigated (speed, velocity, dspeed/dt, acceleration), x_i(t) is the temporal profile of the i-th variable, and each of these variables are convolved with an exponential kernel of amplitude a_i and time constant τ_i. This choice was motivated by the fact that single neuron and

population dynamics showed long lasting responses. For each PC, we fitted the corresponding values of a_i and τ_i by minimizing the square difference between the measured population dynamics and $y(t)$. Analogously with what described for cross validated PCA, fits were performed on a training set, validation was measured on a test set, the procedure was repeated 10 times with random realizations of training and test sets, and the mean and standard error of the predictor performance (measured with R^2) were evaluated averaging over realizations. In V1 and the pulvinar, the model captures a large amount of variance in the first 4 PCs (97.2±0.2, 96.2±0.7, 93.7±2.0, and 88.0±1.3 in V1; and 95.9±0.9, 93.3±1.1, 85.5±4.0, and 80.5±4.8 in the pulvinar), but then much less in other PCs (55.7±4.0 in V1 and 18.1±17.8 in the pulvinar).

Trial to trial variability in the single neuron responses affected our estimates of firing rates and led to different dynamics along each PC in the training and the test sets. These fluctuations are due to the finite number of trials in the experiments; hence they could not be captured by our "kernel" model described above, but can strongly influence our estimate of its performance. To account for this phenomenon in our quantification of the predictor performance, we defined a "null model", which used the dynamics observed in the training set as predictor for the dynamics along each PC in the test set. This null model quantifies the reliability of our estimate of firing rates. It was used as a reference to evaluate the performance of the "kernel" model. Specifically, in each PC we computed the proportion of the variance in the test set explained by the null model (measured with R^2). A value R^2 close to 1 indicates that the estimate of the firing rate of cells was reliable across training and test sets; a value close to zero or negative, on the other hand, indicates that our estimates of firing rates were mainly determined by trial to trial fluctuations. We found that the null model in V1 and the pulvinar had a positive R^2 only for the first 5 and 6 components, respectively. For PCs with positive R^2, we computed the ratio between R^2 given by the kernel model and the null model; this ratio, which we called the fraction of explainable variance captured, is shown in the bar plots of Figures 1C and 2C.

To estimate the importance of the i-th variable, we repeated the procedure described above, setting a_j =0 for all $j \neq i$. The analysis in V1 revealed that the first PC was mostly explained by speed and its derivative (Kernel time constants 0.219±0.004s and 5.0±0.1s); the second PC was mostly explained by velocity and acceleration (kernel time constants 8.56±0.05ms and 4.8±0.1s); while the third PC was mostly related to speed and its time derivative (kernel time constants 2.62±0.03s and 0.674±0.008s). Similar results were obtained in the pulvinar.

Decoding analysis

Decoding of head movement related information from neural activity was performed by training decoders on spike counts in bins of 100ms. Decoders were trained on 80% of the bins and tested on the remaining 20%. Figures in the manuscript only show decoder predictions on test bins. To evaluate performance of decoders, training and testing were repeated 100 times, randomly shuffling which trials were used for training and for testing. Decoding performance with shuffled labels were evaluated using the same procedure, but shuffling the association between spikes in a bin and the corresponding animal head movement. Numerical analyses were performed using the python library scikit-learn.

Logistic regression models (solver 'lbfgs' and 'l2' regularization)[43] were used to decode head movement direction. To quantify the history dependent movement response, we trained separate decoders for each bin to predict if the corresponding trial was CW or CCW. Training was performed assigning sample weight to each movement value (CW or CCW) that corresponded to its frequency in the dataset. The regularization parameter C of each decoder was determined by maximizing the cross validated performance. Generalization performance across movement profiles was measured using a unique logistic regression model for all the time bins along the trial.

Velocity and acceleration decoding were performed using a nonlinear decoder constructed combining a logistic regression model predicting instantaneous movement direction (three categories: no movement, CW, CCW) and two distinct ridge regression models (corresponding to bins with CW and CCW movements) predicting instantaneous movement magnitude. Unlike those used to characterize history dependent effects, the logistic regression models used here were unique for all the time bins along the trial. The ‘l2' regularization parameter of the ridge regression model was optimized to maximize cross validation performance. Training was performed assigning sample weight to each data point; these were computed dividing possible head movement values in 30 equally spaced bins and measuring the frequency of each movement bin in the dataset. We found that this nonlinear decoder outperformed a simpler linear decoder, obtained with a single ridge regression model; this result was likely due to the fact that, unlike the linear decoder, the nonlinear decoder was able to exploit cells with symmetric CCW and CW response.

To evaluate performance of decoders as a function of the number of cells, we systematically measured decoding performance as a function of the number of neurons the decoder had access to. For a fixed number of neurons, this was implemented by randomly picking which neurons were used in the decoding and repeating the procedure 1000 times. Mean and standard error of the decoding performance over random realizations of the training and test set are shown in Figures 1D-F, S2B-D, 2D-F, and S3E,F.

Acknowledgments

We thank Pooja Saraf, Qui Ying Wu, and Leo Ruan for technical assistance, the former and current members of the Scanziani lab for discussions, and the member of the SensoMotion lab for critical reading of the manuscript.

Funding

National Institutes of Health grants U19NS107613 (MS), R01EY025668 (MS), U01NS108683 (AS and NB) and Howard Hughes Medical Institute (MS).

Author contributions

G.B. and M.S. designed experiments. G.B., A.S., N.B., and M.S. wrote the manuscript. G.B. performed all experiments, except that E.H. processed the tissues for tracing experiments. G.B. and A.S. analyzed the data. A.S. performed all the principal component and decoding analysis.

Bibliography

1. Angelaki, D.E., Gu, Y., and Deangelis, G.C. (2011). Visual and vestibular cue integration for heading perception in extrastriate visual cortex. J Physiol *589*, 825–833. https://doi.org/10.1113/jphysiol.2010.194720.
2. Cullen, K.E., and Taube, J.S. (2017). Our sense of direction: progress, controversies and challenges. Nat Neurosci *20*, 1465–1473. https://doi.org/10.1038/nn.4658.
3. Duffy, C.J. (1998). MST neurons respond to optic how and translational movement. J Neurophysiol *80*, 1816–1827. https://doi.org/10.1152/jn.1998.80.4.1816.
4. Magnin, G.V.-M., and M. (1982). Single Neuron Activity Related to Natural Vestibular Stimulation in the Cat's Visual Cortex. Exp Brain Res, 451–455.
5. Rancz, E.A., Moya, J., Drawitsch, F., Brichta, A.M., Canals, S., and Margrie, T.W. (2015). Widespread vestibular activation of the rodent cortex. Journal of Neuroscience *35*, 5926–5934. https://doi.org/10.1523/JNEUROSCI.1869-14.2015.
6. Hennestad, E., Witoelar, A., Chambers, A.R., and Vervaeke, K. (2021). Mapping vestibular and visual contributions to angular head velocity tuning in the cortex. Cell Rep *37*, 110134. https://doi.org/10.1016/j.celrep.2021.110134.
7. Bouvier, G., Senzai, Y., and Scanziani, M. (2020). Head Movements Control the Activity of Primary Visual Cortex in a Luminance-Dependent Manner. Neuron *108*, 500-511.e5. https://doi.org/10.1016/j.neuron.2020.07.004.
8. Vélez-Fort, M., Bracey, E.F., Keshavarzi, S., Rousseau, C. V., Cossell, L., Lenzi, S.C., Strom, M., and Margrie, T.W. (2018). A Circuit for Integration of Head- and Visual-Motion Signals in Layer 6 of Mouse Primary Visual Cortex. Neuron *98*, 179-191.e6. https://doi.org/10.1016/j.neuron.2018.02.023.
9. Keshavarzi, S., Bracey, E.F., Faville, R.A., Campagner, D., Tyson, A.L., Lenzi, S.C., Branco, T., and Margrie, T.W. (2022). Multisensory coding of angular head velocity in the retrosplenial cortex. Neuron *110*, 532-543.e9. https://doi.org/10.1016/j.neuron.2021.10.031.
10. Van Alphen, A.M., Stahl, J.S., and De Zeeuw, C.I. (2001). The dynamic characteristics of the mouse horizontal vestibulo-ocular and optokinetic response. Brain Res *890*, 296–305. https://doi.org/10.1016/S0006-8993(00)03180-2.
11. Miura, S.K., and Scanziani, M. (2022). Distinguishing externally from saccade-induced motion in visual cortex. Nature. https://doi.org/10.1038/s41586-022-05196-w.
12. Itokazu, T., Hasegawa, M., Kimura, R., Osaki, H., Albrecht, U.R., Sohya, K., Chakrabarti, S., Itoh, H., Ito, T., Sato, T.K., et al. (2018). Streamlined sensory motor communication through cortical reciprocal connectivity in a visually guided eye movement task. Nat Commun *9*. https://doi.org/10.1038/s41467-017-02501-4.
13. Pisano, T.J., Dhanerawala, Z.M., Kislin, M., Bakshinskaya, D., Engel, E.A., Lee, J., de Oude, N.L., Hansen, E.J., Venkataraju, K.U., Hoebeek, F.E., et al. (2021). Parallel Organization of Cerebellar Pathways to Sensory, Motor, and Associative Forebrain. Cell Rep *36*, 109721. https://doi.org/10.2139/ssrn.3810000.
14. Kebschul, J.M., Richman, E.B., Ringach, N., Friedmann, D., Albarran, E., Kolluru, S.S., Jones, R.C., Allen, W.E., Wang, Y., Cho, S.W., et al. (2020). Cerebellar nuclei evolved by repeatedly duplicating a conserved cell-type set. Science (1979) *370*. https://doi.org/10.1126/science.abd5059.

15. Fujita, H., Kodama, T., and du Lac, S. (2020). Modular output circuits of the fastigial nucleus mediate diverse motor and nonmotor functions of the cerebellar vermis. Elife, 1–36. https://doi.org/10.1101/2020.04.23.047100.
16. Liang, Y., Fan, J.L., Sun, W., Lu, R., Chen, M., and Ji, N. (2021). A Distinct Population of L6 Neurons in Mouse V1 Mediate Cross-Callosal Communication. Cerebral Cortex *31*, 4259–4273. https://doi.org/10.1093/cercor/bhab084.
17. Weiler, S., Teichert, M., and Margrie, T.W. (2024). Layer 6 corticocortical cells dominate the anatomical organization of intra and interhemispheric feedback. https://doi.org/10.1101/2024.05.01.590702.
18. Lien, A.D., and Scanziani, M. (2013). Tuned thalamic excitation is amplified by visual cortical circuits. Nat Neurosci *16*, 1315–1323. https://doi.org/10.1038/nn.3488.
19. Guo, Z. V., Li, N., Huber, D., Ophir, E., Gutnisky, D., Ting, J.T., Feng, G., and Svoboda, K. (2014). Flow of cortical activity underlying a tactile decision in mice. Neuron *81*, 179–194. https://doi.org/10.1016/j.neuron.2013.10.020.
20. Li, N., Chen, S., Guo, Z. V., Chen, H., Huo, Y., Inagaki, H.K., Chen, G., Davis, C., Hansel, D., Guo, C., et al. (2019). Spatiotemporal constraints on optogenetic inactivation in cortical circuits. Elife *8*, 1–31. https://doi.org/10.7554/eLife.48622.
21. Niell, C.M., and Stryker, M.P. (2010). Modulation of Visual Responses by Behavioral State in Mouse Visual Cortex. Neuron *65*, 472–479. https://doi.org/10.1016/j.neuron.2010.01.033.
22. Stringer, C., Pachitariu, M., Steinmetz, N., Reddy, C.B., Carandini, M., and Harris, K.D. (2019). Spontaneous behaviors drive multidimensional, brainwide activity. Science *364*. https://doi.org/10.1126/science.aav7893.
23. Deneux, T., Harrell, E.R., Kempf, A., Ceballo, S., Filipchuk, A., and Bathellier, B. (2019). Context-dependent signaling of coincident auditory and visual events in primary visual cortex. Elife *8*, 1–23. https://doi.org/10.7554/eLife.44006.
24. Bimbard, C., Sit, T.P.H., Lebedeva, A., Reddy, C.B., Harris, K.D., and Carandini, M. (2023). Behavioral origin of sound-evoked activity in mouse visual cortex. Nat Neurosci *26*, 251–258. https://doi.org/10.1038/s41593-022-01227-x.
25. Oude Lohuis, M.N., Marchesi, P., Olcese, U., and Pennartz, C.M.A. (2024). Triple dissociation of visual, auditory and motor processing in mouse primary visual cortex. Nat Neurosci *27*, 758–771. https://doi.org/10.1038/s41593-023-01564-5.
26. Faulstich, B.M., Onori, K.A., and Du Lac, S. (2004). Comparison of plasticity and development of mouse optokinetic and vestibulo-ocular reflexes suggests differential gain control mechanisms. Vision Res *44*, 3419–3427. https://doi.org/10.1016/j.visres.2004.09.006.
27. Juavinett, A.L., Kim, E.J., Collins, H.C., and Callaway, E.M. (2020). A systematic topographical relationship between mouse lateral posterior thalamic neurons and their visual cortical projection targets. Journal of Comparative Neurology *528*, 95–107. https://doi.org/10.1002/cne.24737.
28. Scholl, L.R., Foik, A.T., and Lyon, D.C. (2021). Projections between visual cortex and pulvinar in the rat. Journal of Comparative Neurology *529*, 129–140. https://doi.org/10.1002/cne.24937.
29. Roth, M.M., Dahmen, J.C., Muir, D.R., Imhof, F., Martini, F.J., and Hofer, S.B. (2016). Thalamic nuclei convey diverse contextual information to layer 1 of visual cortex. Nat Neurosci *19*, 299–307. https://doi.org/10.1038/nn.4197.
30. Bennett, C., Gale, S.D., Garrett, M.E., Newton, M.L., Callaway, E.M., Murphy, G.J., and Olsen, S.R. (2019). Higher-Order Thalamic Circuits Channel Parallel Streams of

Visual Information in Mice. Neuron *102*, 477-492.e5. https://doi.org/10.1016/j.neuron.2019.02.010.

31. Wang, Q., and Burkhalter, A. (2007). Area map of mouse visual cortex. Journal of Comparative Neurology *502*, 339–357. https://doi.org/doi:10.1002/cne.21286.
32. Siegle, J.H., Jia, X., Durand, S., Gale, S., Bennett, C., Graddis, N., Heller, G., Ramirez, T.K., Choi, H., Luviano, J.A., et al. (2021). Survey of spiking in the mouse visual system reveals functional hierarchy. Nature *592*, 86–92. https://doi.org/10.1038/s41586-020-03171-x.
33. Honnuraiah, S., Huang, H., Ryan, W.J., Broersen, R., Connelly, W.M., Stuart, G.J., and Stuart, G. Cellular and circuit mechanisms underlying binocular vision. https://doi.org/10.1101/2024.03.11.584536.
34. Hitier, M., Besnard, S., and Smith, P.F. (2014). Vestibular pathways involved in cognition. Front Integr Neurosci *8*, 1–16. https://doi.org/10.3389/fnint.2014.00059.
35. Meng, H., and Angelaki, D.E. (2010). Responses of Ventral Posterior Thalamus Neurons to Three-Dimensional Vestibular and Optic Flow Stimulation. J Neurophysiol *103*, 817–826. https://doi.org/10.1152/jn.00729.2009.
36. Leow, Y.N., Zhou, B., Sullivan, H.A., Barlowe, A.R., Wickersham, I.R., and Sur, M. (2022). Brain-wide mapping of inputs to the mouse lateral posterior (LP/Pulvinar) thalamus–anterior cingulate cortex network. Journal of Comparative Neurology *530*, 1992–2013. https://doi.org/10.1002/cne.25317.
37. Brenner, J.M., Beltramo, R., Gerfen, C.R., Ruediger, S., and Scanziani, M. (2023). A genetically defined tecto-thalamic pathway drives a system of superior-colliculus-dependent visual cortices. Neuron *111*, 2247-2257.e7. https://doi.org/10.1016/j.neuron.2023.04.022.
38. Furutachi, S., Franklin, A.D., Aldea, A.M., Mrsic-Flogel, T.D., and Hofer, S.B. (2024). Cooperative thalamocortical circuit mechanism for sensory prediction errors. Nature *633*, 398–406. https://doi.org/10.1038/s41586-024-07851-w.
39. Zingg, B., Chou, X. lin, Zhang, Z. gang, Mesik, L., Liang, F., Tao, H.W., and Zhang, L.I. (2017). AAV-Mediated Anterograde Transsynaptic Tagging: Mapping Corticocollicular Input-Defined Neural Pathways for Defense Behaviors. Neuron *93*, 33–47. https://doi.org/10.1016/j.neuron.2016.11.045.
40. Liu, B.H., Huberman, A.D., and Scanziani, M. (2016). Cortico-fugal output from visual cortex promotes plasticity of innate motor behaviour. Nature *538*, 383–387. https://doi.org/10.1038/nature19818.
41. Senzai, Y., Fernandez-Ruiz, A., and Buzsáki, G. (2019). Layer-Specific Physiological Features and Interlaminar Interactions in the Primary Visual Cortex of the Mouse. Neuron *101*, 500-513.e5. https://doi.org/10.1016/j.neuron.2018.12.009.
42. McInnes, L., Healy, J., and Melville, J. (2018). UMAP: Uniform Manifold Approximation and Projection for Dimension Reduction. https://doi.org/https://doi.org/10.48550/arXiv.1802.03426.
43. Pedregosa, F., Michel, V., Grisel, O., Blondel, M., Prettenhofer, P., Weiss, R., Vanderplas, J., Cournapeau, D., Varoquaux, G., Gramfort, A., et al. (2011). Scikit-learn: Machine Learning in Python.

Supplementary Figures

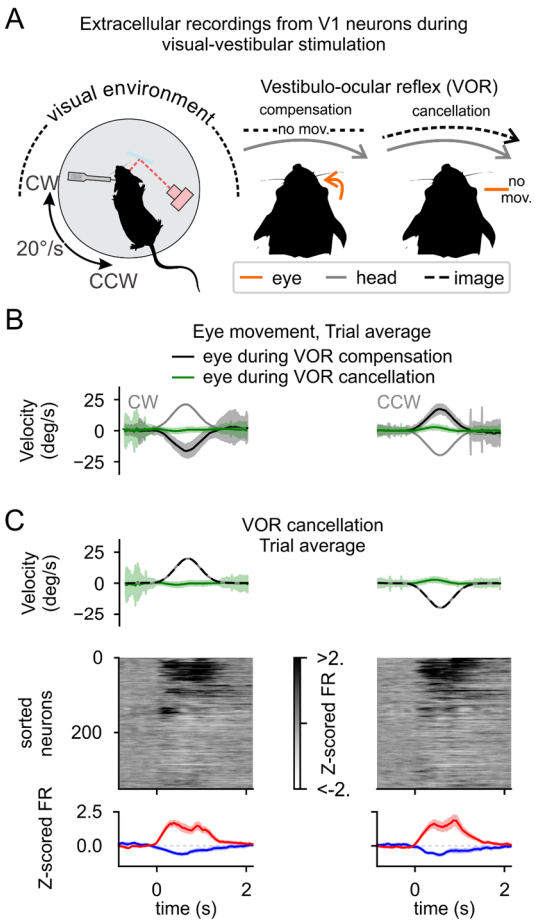

Figure S1. V1 neurons respond to head movements with or without compensatory eye movements, related to Figure 1.

(A) Experimental configuration. Extracellular linear probe in the left V1 of a head-fixed, awake mouse records the response to clockwise (CW) and counterclockwise (CCW) rotations of the table surrounded by a virtual drum (dotted line). To minimize the number of fast compensatory eye movements, we use a lower velocity peak amplitude: 20 deg/s, instead of 80 deg/s used in all other experiments (see Methods).

(B) Vestibulo-ocular reflex (VOR) under two conditions: compensation (black) and cancellation (green). A VOR gain of 1 (ratio of 1 between eye and head movement) indicates perfect VOR compensation, while a VOR gain of 0 indicates perfect VOR cancellation. The gray line shows the head movement velocity profile.

(C) Velocity profiles (top): Head velocity (gray), eye velocity (green), and image (visual environment) velocity (dotted line). While rotating the animal, the comoving visual stimulation triggered a VOR cancellation (VOR gain = 0.09±0.04, same trace as in B). UMAP sorting of the averaged Z-scored FR responses across neurons performing CW (left) and CCW (right) head movements (middle). Z-scored average of the firing rate for the neurons that are significantly excited (red) and suppressed (blue) (bottom).

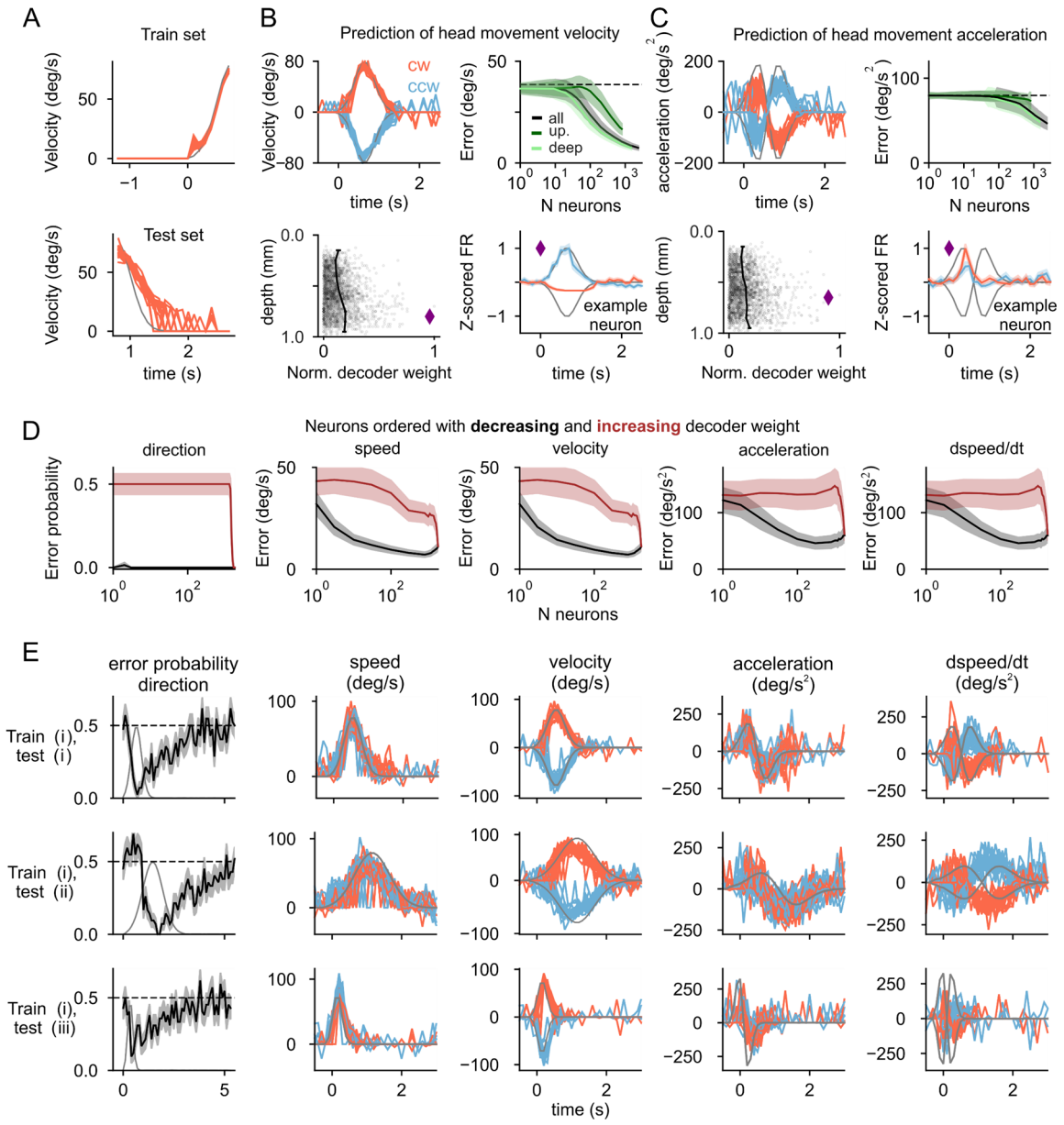

Figure S2. Prediction of head movement velocity and acceleration and generalization of head movement information to different head angular rotation profiles, related to Figure 1.

(A) Prediction of head velocity of a decoder trained on the rising phase (top) and tested on the decaying phase (bottom) of the head movement profile.

(B) Instantaneous head angular velocity representation: Prediction of head movement velocity (top left), error as a function of number of neurons (top right), decoder weight of single neuron as a function of depth (bottom left), and example neuron selected using highest decoder weight for head angular speed decoding (bottom right). As in Figure 1D, light and dark green indicate deep and superficial layers, respectively.

(C) As in B but for time derivative of velocity (acceleration).

(D) Decoding error of head movement as a function of number of neurons. To obtain these plots, starting from the decoding weight obtained when all neurons are available (e.g. those shown in Figure 1 C,D of the main text and in panels A,B of the current figure), we arrange

neurons in decreasing (black) and increasing (red) order of the decoder weight. The errors shown for a given N in the plots are those obtained from a decoder which has access to the first N neurons according to this ordering.
(E) Instantaneous head movement direction predicted by a decoder trained on profiles with 80 deg/s peak velocity and tested on other velocity profiles with the same peak velocity but with slower (middle) and faster (bottom) profiles.
Example neurons in panels A-C are marked with purple diamonds. In A-C and E, blue and red traces correspond to quantities measured during CCW and CW rotations, respectively.

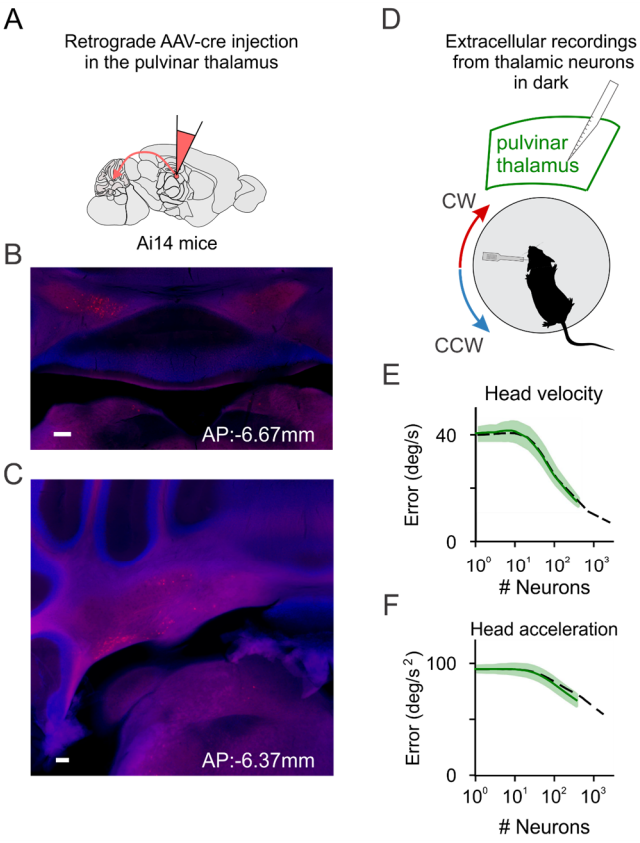

Figure S3. The pulvinar receives projections from the deep cerebellar nuclei and encodes head angular velocity and acceleration, related to Figure 2.
(A) Experimental strategy (top). Injection of Cre dependent retrograde virus (rAAV2.1 hSyn-cre) in the rostro-medial pulvinar in a flex-tdTomato reporter line; this approach labels the neurons that project to the pulvinar.
(B, C) Deep cerebellar and vestibular nuclei coronal slice at -6.67mm (B) and -6.37mm (C) from Bregma. DAPI is in blue and td-Tomato is red.
(D) Experimental configuration (top). Extracellular linear probe in ipsilateral pulvinar (green) or in V1 (black) of a head-fixed, awake mouse records the response to CW (red) and CCW (blue) rotations of the table in the dark.
(E) Decoding error of head movement angular velocity as a function of number of neurons in pulvinar (green) and V1 (black).
(F) As in E but for head movement acceleration.
Scale bar = 200 μm in B and C.